









# A debris-covered glacier at Kerguelen (49°S, 69°E) over the past 15 000 years

JOANNA CHARTON <sup>1,2</sup>, VINCENT JOMELLI <sup>1,2</sup>, IRENE SCHIMMELPFENNIG <sup>2</sup>,  
DEBORAH VERFAILLIE <sup>3</sup>, VINCENT FAVIER <sup>4</sup>, FATIMA MOKADEM<sup>1</sup>, ADRIEN GILBERT <sup>4</sup>,  
FANNY BRUN <sup>4</sup>, GEORGES AUMAÎTRE<sup>2,5</sup>, DIDIER L. BOURLÈS <sup>2,5</sup> and KARIM KEDDADOUCHE<sup>2,5</sup>

<sup>1</sup>Université Paris 1 Panthéon-Sorbonne, CNRS Laboratoire de Géographie Physique, 92195 Meudon, France

<sup>2</sup>Aix-Marseille University, CNRS, IRD, INRAE, Collège de France, UM 34 CEREGE, 13545 Aix-en-Provence, France

<sup>3</sup>Earth and Life Institute, Université catholique de Louvain, B-1348 Louvain-la-Neuve, Belgium

<sup>4</sup>Université Grenoble Alpes, IGE, CNRS, 38058 Grenoble, France

<sup>5</sup>ASTER Team

[joanna.charton@gmail.com](mailto:joanna.charton@gmail.com)

**Abstract:** Debris-covered glaciers constitute a large part of the world's cryosphere. However, little is known about their long-term response to multi-millennial climate variability, in particular in the Southern Hemisphere. Here, we provide first insights into the response of a debris-covered glacier to multi-millennial climate variability in the sub-Antarctic Kerguelen Archipelago, which can be compared to that of recently investigated debris-free glaciers. We focus on the Gentil Glacier and present 13 new <sup>36</sup>Cl cosmic-ray exposure ages from moraine boulders. The Gentil Glacier experienced at least two glacial advances: the first one during the Late Glacial (19.0–11.6 ka) at ~14.3 ka and the second one during the Late Holocene at ~2.6 ka. Both debris-covered and debris-free glaciers advanced broadly synchronously during the Late Glacial, most probably during the Antarctic Cold Reversal event (14.5–12.9 ka). This suggests that both glacier types at Kerguelen were sensitive to abrupt temperature changes recorded in Antarctic ice cores, associated with increased moisture. However, during the Late Holocene, the advance at ~2.6 ka was not observed in other glaciers and seems to be an original feature of the debris-covered Gentil Glacier, related to either distinct dynamics or to distinct sensitivity to precipitation changes.

Received 22 April 2020, accepted 7 September 2020

**Key words:** Antarctic Cold Reversal, glacier fluctuations, Holocene, *in situ* cosmogenic chlorine-36 dating, palaeoclimate, sub-Antarctic

## Introduction

Debris-covered glaciers exhibit a debris-mantled glacial tongue, with rock debris ranging from a few centimetres to several metres in thickness (Mayr & Hagg 2019). This type of glacier constitutes a substantial proportion of the glaciers worldwide, both in the Northern and Southern Hemispheres (Scherler *et al.* 2018). Therefore, several recent investigations have been conducted on debris-covered glaciers in order to document their surface changes (Vincent *et al.* 2016, Brun *et al.* 2018), as well as the morphological (Salerno *et al.* 2017, Brun *et al.* 2019) and climatic factors (Ojha *et al.* 2017) controlling their spatial distribution and response to climate fluctuations. It has been previously suggested that debris-covered glaciers are less sensitive to climatic variation than debris-free glaciers owing to the thickness of the debris cover, which plays an isolating role and protects the ice from melting by absorbing incoming radiation (Mayr & Hagg 2019). However, recent studies on Himalayan glaciers have shown a similar thinning rate

between debris-free and debris-covered glaciers facing regional pluriannual climatic variations (Kääb *et al.* 2012, Vincent *et al.* 2016, Brun *et al.* 2018, 2019).

However, little is known about the differences in the glacier responses to temperature and precipitation changes over longer timescales. This issue has rarely been investigated, and the sites of all known studies are located in the Northern Hemisphere and subject to alpine climate conditions. To our knowledge, so far only two studies using cosmic-ray exposure (CRE) dating of supraglacial debris were specifically undertaken to constrain the Late Glacial and Holocene history of a fossil debris-covered glacier in Spain (Fernández-Fernández *et al.* 2017) and of debris-covered glacier-rock glacier continua in northern Iceland (Fernández-Fernández *et al.* 2020). Debris-covered glaciers on the Kerguelen Archipelago in the sub-Antarctic region offer an excellent opportunity to document their evolution related to long-term regional and global climate changes. Moreover, recent chronologies of debris-free glaciers are available in different glacial valleys of the

archipelago (Jomelli *et al.* 2017, 2018). This work presents 13 new  $^{36}\text{Cl}$  CRE ages from boulders collected on two sets of frontal morainic ridges (G1, G2) from Gentil Glacier, a debris-covered glacier located in the south of Kerguelen Archipelago. We then compare the evolution of Gentil Glacier to the evolution of the nearby debris-free glaciers investigated in previous studies (Jomelli *et al.* 2017, 2018).

## Study area

The French Kerguelen Archipelago is located in the southern Indian Ocean (49°S) and constitutes a 40 million year-old part of an underwater basaltic plateau that has emerged. The archipelago is of major regional interest because it is the largest above-water glaciated area of the sub-Antarctic (552 km<sup>2</sup>; Berthier *et al.* 2009). It is one of the few places in the Indian Ocean where glacial records are available, besides Heard Island (e.g. Thost & Truffer 2008) and the recently investigated Marion Islands (Rudolph *et al.* 2020). Cook Ice Cap (CIC; 410 km<sup>2</sup> in 2001) is the largest glaciated area on Kerguelen Archipelago with marine and terrestrial termini. It deposited several glacial moraines on the eastern part of the main island, called Grande Terre, which were previously investigated (Jomelli *et al.* 2017, 2018). Smaller debris-free mountain glaciers are also present in different sectors of the archipelago: on Rallier du Baty Peninsula, in Presqu'île de la Société de Géographie and on Gallieni Peninsula (Fig. 1).

Kerguelen has an oceanic subpolar climate characterized by a low seasonality in temperature and precipitation. The annual mean temperature is ~4.5°C and precipitation is ~800 mm per year on the eastern side of the archipelago, whereas the western side receives up to 4000 mm per year (Favier *et al.* 2016, Verfaillie *et al.* 2019). A permanent weather station has been continuously maintained since 1951 at the scientific station based at Port-aux-Français on Coubert Peninsula.

The debris-covered Gentil Glacier is an active glacier on Gallieni Peninsula, which is located in the south of the main island and is dominated by Mount Ross (1850 m above sea level (a.s.l.)), the highest peak of the archipelago (Fig. 1). Mount Ross is a strato-volcano in which the caldera formed a glacial cirque from which Buffon Glacier flows down on its western slope and reaches the sea (Fig. 1b). Gentil Glacier constitutes a glacial lobe of Buffon Glacier and is covered by debris over its entire ablation area. Glacier cross-sections exposed at the numerous ice cliffs (Figs 2a & 3c) indicate debris thicknesses ranging from ~20 cm up to 50–100 cm. Debris cover on the glacier originates from rockslides along the cirque headwalls, avalanches and subglacial bedrock erosion (Fig. 2a). In addition, supraglacial debris

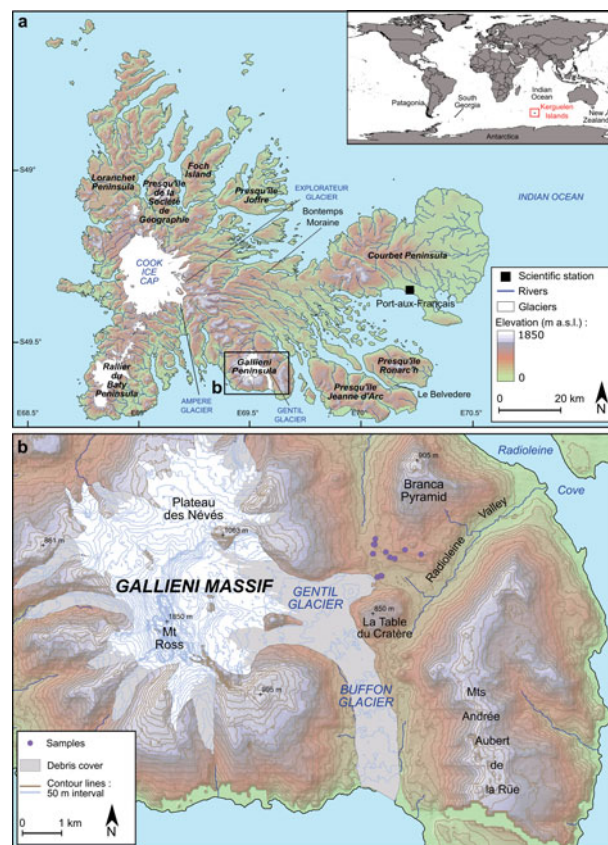


**Fig. 1.** a. Map of the Kerguelen Archipelago and its location. b. The study area, Gentil Glacier, on Gallieni Peninsula, in the south of the archipelago (Digital Elevation Model from <https://lpdaac.usgs.gov/products/astgtmv003>, glacier outlines from the Global Land Ice Measurement from Space (GLIMS) database; Raup *et al.* 2007).

is laterally supplied from the catchment slopes and lateral moraines during the downstream flow of the glacier. As a result, the glacier transports subglacial and supraglacial debris, which is concentrated by the glacial flow into discrete subparallel lateral and frontal layered ridges atop the glacier (Figs 2 & 3a). At the glacier's snout, the debris bulges isolate the subjacent ice and then form ice-cored moraines that are concentrically deposited following the delineation of the glacier (also called 'controlled moraine'; e.g. Evans 2009). Three geomorphological features can be distinguished (Fig. 2): 1) an active part that is still fed by ice flow (where the investigated G2 moraine set is located), 2) an inactive part that is characterized by an ice-cored moraine layer that does not seem to be connected with the ice flow anymore (pink swath in Fig. 2), and 3) the fossil part, where the ice has melted completely and only vegetated glacial moraine deposits remain (where the investigated G1 moraine set is located). In both active and inactive areas, the debris mantle surface is hilly and characterized by numerous ice cliffs and supraglacial lakes (Fig. 3a & 3c). The fossil part is

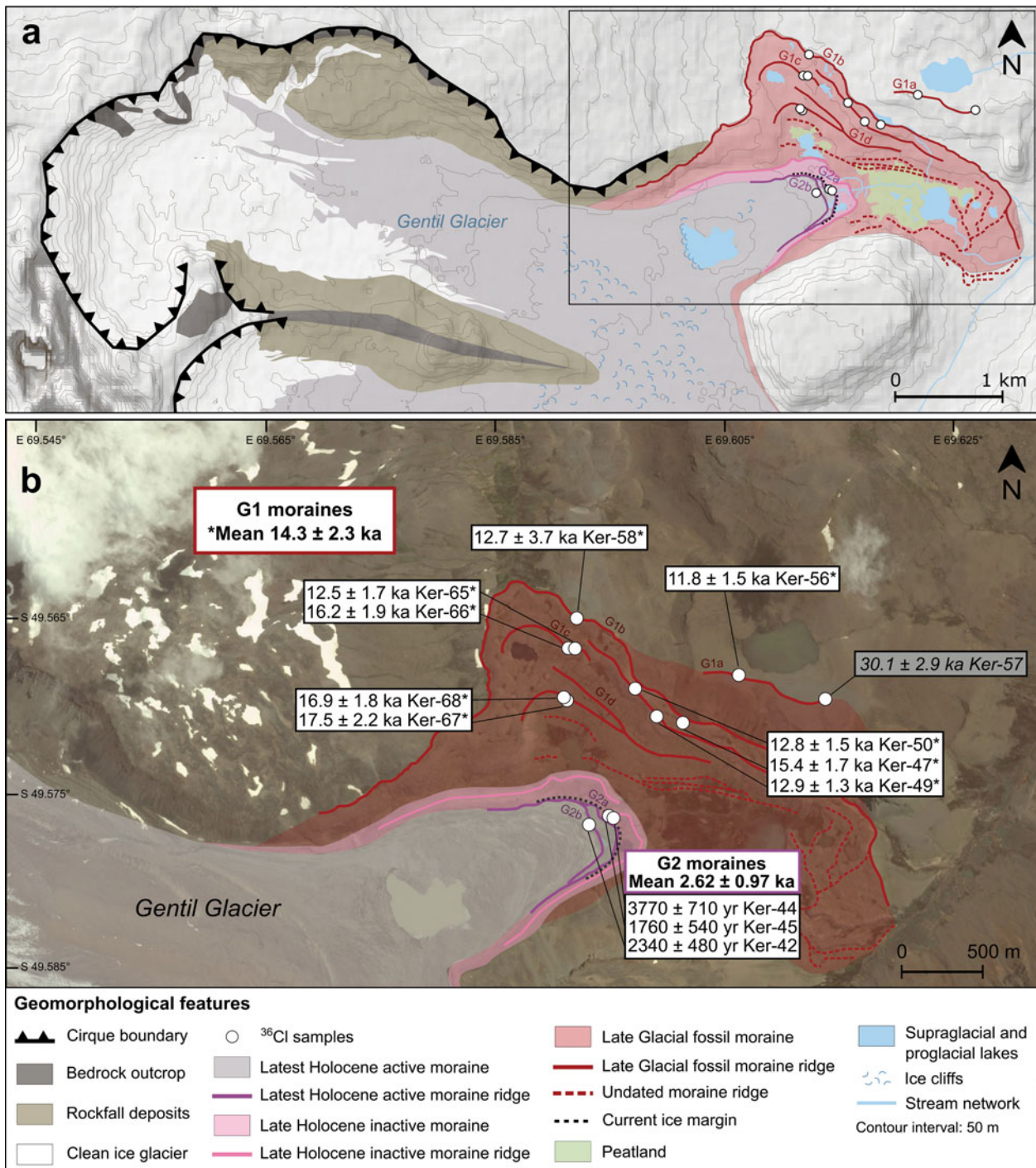


**Fig. 2.** a. Glacial geomorphological map of Gentil Glacier, Kerguelen Archipelago. Rectangle corresponds to limits of **b.**, which shows aerial imagery of the study area with geomorphological features. White boxes show the <sup>36</sup>Cl ages of the moraine boulders with their inferred analytical uncertainties. <sup>36</sup>Cl age in italics (Ker-57) is rejected as a statistical outlier and therefore excluded from the discussion. The asterisks mark the ages that are included in the arithmetic mean age of the G1 moraine group. The arithmetic mean ages of both moraine groups are shown with their full errors (i.e. standard deviation, analytical and production rate uncertainties).

characterized by a near-continuous, hummocky rock pavement that is very similar to the current detrital cover of the glacier (Fig. 3b). Therefore, we assume that the

glacier was already covered during one of its last advances and that this rocky pavement corresponds to the former debris cover.

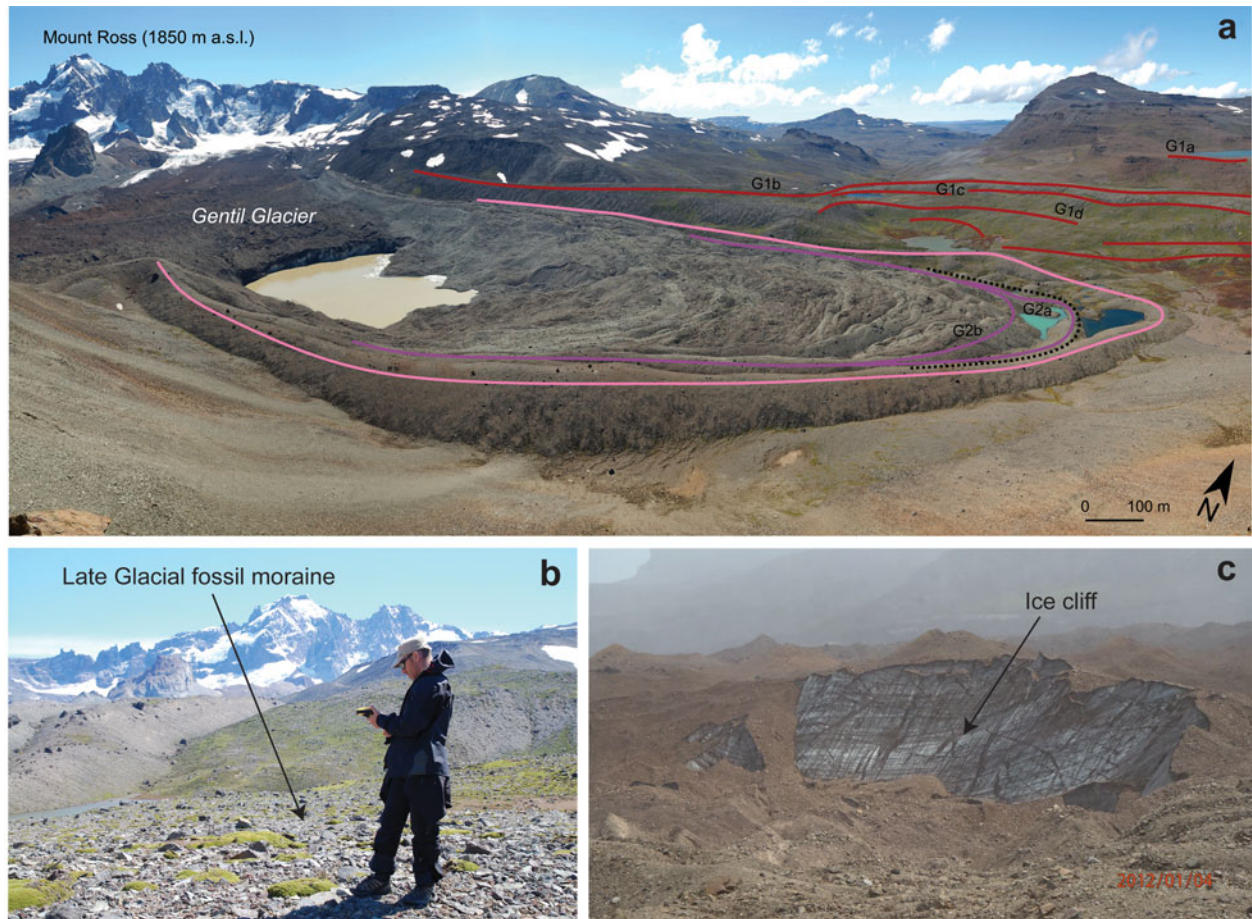


**Fig. 3. a.** Photograph of active debris-covered Gentil Glacier, with the latest Holocene moraine ridges (G2a, G2b; purple lines), the inactive Late Holocene moraine ridge (pink line) and the fossil Late Glacial Period moraine ridges (G1a to G1d; red lines). **b.** Photograph of the fossil G1 Late Glacial Period moraine deposit. **c.** Photograph of one of the numerous ice cliffs, which are present on the active debris surface of Gentil Glacier.

### Previous studies on Kerguelen glaciers

Recent investigations conducted on Kerguelen glaciers have shown a significant retreat of debris-free glaciers on the archipelago in recent decades, in particular for CIC, which lost 20% of its surface from 1963 to 2001 (Berthier *et al.* 2009). Direct surface mass balance and energy balance measurements combined with satellite image analyses revealed an even more drastic shrinkage over the last decade (Verfaillie *et al.* 2015, Favier *et al.* 2016). The current CIC wastage is mainly attributed to an atmospheric drying since 1960 caused by a shift of the storm track (positive phase of the Southern Annular Mode (SAM); Favier *et al.* 2016) due to the greenhouse gas concentration increase and the Antarctic ozone hole (Thompson *et al.* 2011).

In addition, long-term palaeoglacier changes have been investigated through  $^{36}\text{Cl}$  dating. At  $\sim 40$  ka (i.e. during Marine Isotopic Stage 3 (MIS 3)), glaciers covered a greater part of the archipelago, and  $^{36}\text{Cl}$  chronologies

obtained from moraines and erratic boulders revealed that CIC outlet glaciers were generally retreating from  $\sim 40$  to  $\sim 15$  ka (Jomelli *et al.* 2017, 2018). This indirectly implies that Kerguelen glaciers might have experienced an early local Last Glacial Maximum during MIS 3, in agreement with recent findings on Marion Island (Rudolph *et al.* 2020). The deglaciation trend was interrupted  $\sim 15$ – $12$  ka in at least two locations on the archipelago, probably during the Antarctic Cold Reversal (ACR; Jomelli *et al.* 2017, 2018). One of the locations revealing a glacial advance or stillstand at this time is the Bontemps moraine dated at  $13.6 \pm 1.5$  ka. It is located 26 km from the current ice margin of Explorateur Glacier on the eastern slope of CIC (Fig. 1). The other location is the Belvedere moraine situated 2.7 km from the watershed crest and dated at  $15.5 \pm 1.8$  ka (Fig. 1).

There is little evidence of glacial fluctuations during the Holocene period, apart from radiocarbon ages (Frenot *et al.* 1997) and  $^{36}\text{Cl}$  ages from the Ampere Glacier proglacial margin (Jomelli *et al.* 2017), located on the

southern slope of CIC (Fig. 1). The current glacial retreat of Ampere Glacier uncovered peat bogs upstream of Ampere Lake, from which samples were radiocarbon dated to the Early, Mid and Late Holocene, probably attesting to the presence of smaller glaciers during most of the Holocene period than during the last millennium (Frenot *et al.* 1997). During this time, Ampere Glacier experienced a last advance, which overlaid the peatland and formed a series of moraines, including one dated to  $1310 \pm 320$  CE (Jomelli *et al.* 2017).

## Methods

### Sampling

Fieldwork was conducted in January 2012 in the Radioleine glacial valley, on the eastern slope of Mount Ross (Fig. 1b). Thirteen samples were collected on moraine boulders from two groups of moraines (G1 and G2; Figs 2 & 3) that were identified as Gentil Glacier's morainic deposits. As Gentil Glacier is a debris-covered glacier, morainic deposits originate from supraglacial and subglacial rock materials, which are transported atop the ice by the ice flow (Evans 2009). Thus, boulders that were sampled for  $^{36}\text{Cl}$  dating might already have been exposed at the surface for an unknown duration of time before moraine formation. Moreover, chaotic topography at the glacier surface and heterogeneous rock debris thickness may cause variation in the exposure to the cosmic-ray flux due to the possible rotation of the boulders or burying, as observed on the active part of the glacier. In addition, moraines that were deposited at the glacier terminus (at both the active or inactive areas) are still ice-cored. Therefore, further ice movements and melting processes have certainly occurred locally, even after moraine formation. Thus, each boulder has its own exposure and stability history (Heyman *et al.* 2011). The specific character of these glacial moraines has several implications that differ from the investigation of debris-free glacier moraines:

- 1) Moraine ridges on the still-active part of the glacier indicate that the glacier advanced at some time in the past, but these ridges are not yet stabilized, because after the glacier advance, the insulating debris cover prevents the ice from melting for several millennia.
- 2) Some variability in the  $^{36}\text{Cl}$  ages may be observed from a single landform due to boulder pre-exposure during supraglacial transport and post-depositional remobilisation of previously exposed boulders (nuclide inheritance), leading to overestimated  $^{36}\text{Cl}$  ages. Moreover, melting of the ice-cored moraine may cause post-depositional rotation or gradual exhumation of boulders that can stretch over several centuries or millennia, causing underestimated  $^{36}\text{Cl}$  ages.

- 3) Each ridge does not necessarily correspond to the front of the glacier at a specific time (i.e. several parallel ridges might have formed during the same glacial advance).

Samples were therefore taken from both the fossil and the active parts of the glacial debris. Each of the two moraine groups sampled in this study is composed of several nearby moraine ridges, which we assume to be formed during the same glacier advance period. We targeted the moraine boulders located on the top of the moraine ridges, thus minimizing the risk of post-depositional rotation and exhumation. The samples were collected with a hammer and chisel from the uppermost ~3–4 cm of flat basaltic boulders, avoiding (as much as possible) edges or eroding surfaces (Fig. 4). A clinometer was used to determine topographical shielding and a handheld global positioning system (GPS) device was used to record geographical coordinates and elevations, which are shown in Table I.

Due to the difficulty of collecting samples and transporting them to the scientific base on Kerguelen without using a helicopter, a limited number of samples were collected. Ten samples were taken from the G1 moraine group located on the fossil moraine deposit at distances of ~0.7 and 1.5 km downstream from the present-day frontal area. G1 is formed by approximately eight moraine ridges, four of which were sampled for



Fig. 4. Photographs of boulders on the fossil G1 moraine sampled during the field campaigns.

**Table I.** Geographical sample locations, topographical shielding factors and sample thicknesses.

| Sample name | Latitude (°S) | Longitude (°E) | Elevation (m) | Shielding factor | Thickness (cm) |
|-------------|---------------|----------------|---------------|------------------|----------------|
| G2          |               |                |               |                  |                |
| Ker-42      | 49.57739      | 69.59248       | 283           | 0.996            | 3              |
| Ker-44      | 49.57704      | 69.59453       | 256           | 0.994            | 3              |
| Ker-45      | 49.57690      | 69.59417       | 265           | 0.992            | 4              |
| G1          |               |                |               |                  |                |
| Ker-47      | 49.57168      | 69.60058       | 338           | 0.998            | 3              |
| Ker-49      | 49.57129      | 69.59832       | 346           | 0.999            | 4              |
| Ker-50      | 49.56972      | 69.59641       | 339           | 0.999            | 4              |
| Ker-56      | 49.56898      | 69.60533       | 407           | 1.000            | 4              |
| Ker-57      | 49.57035      | 69.61282       | 397           | 1.000            | 4              |
| Ker-58      | 49.56575      | 69.59135       | 312           | 0.996            | 4              |
| Ker-65      | 49.56745      | 69.59121       | 204           | 0.998            | 4              |
| Ker-66      | 49.56745      | 69.59066       | 209           | 0.999            | 4              |
| Ker-67      | 49.57031      | 69.59041       | 187           | 0.999            | 4              |
| Ker-68      | 49.57025      | 69.59032       | 186           | 0.999            | 4              |

dating. Ker-56 and -57 were sampled on the most distal moraine ridge (G1a) at ~402 m a.s.l. Ker-47, -49, -50, -58, -65 and -66 were extracted from boulders on two moraine ridges (G1b and G1c) bulged close to the G1a moraine ridge at average altitudes of 341 and 207 m a.s.l., respectively. Ker-67 and -68 were collected on the G1 innermost moraine ridge (G1d) at 187 m a.s.l.

Three samples (Ker-42, -44 and -45) were taken on the two ridges (G2a and G2b) that form the G2 moraine group located on the active moraine deposit (current ice front) at an average altitude of 268 m a.s.l. Field observations were also performed upstream of G1 and G2 in order to find evidence of pumice that would have been deposited at the beginning of the last millennium due to the Allouarn volcanic eruption (Arnaud *et al.*, unpublished data 2016).

#### *In situ-produced <sup>36</sup>Cl CRE dating*

Basaltic whole-rock samples were processed and measured at CEREGE (Aix-en-Provence, France) for *in situ*-produced <sup>36</sup>Cl CRE dating, following the same methods described in Jomelli *et al.* (2017, 2018). Age-calculation methods and parameters are also the same as in these previous studies at Kerguelen. For completeness, details and relevant references are presented in the Supplemental Material, together with the compositional data used for the age calculations (Tables SI & SII). The resulting individual ages are presented in Table II with their 1σ uncertainties, which take into account the full propagation of all uncertainties (analytical and production rate uncertainties). Analytical uncertainties only are also reported in Table II. In order to facilitate

**Table II.** <sup>36</sup>Cl dating results. Spike is enriched in <sup>35</sup>Cl (~99.9%). <sup>36</sup>Cl/<sup>35</sup>Cl and <sup>35</sup>Cl/<sup>37</sup>Cl ratios were inferred from measurements at the ASTER accelerator mass spectrometry facility. Samples in italics were rejected as outliers and excluded from mean age calculations.

| Sample name         | Sample weight (g) | Mass of Cl in spike (mg) | <sup>35</sup> Cl/ <sup>37</sup> Cl | <sup>36</sup> Cl/ <sup>35</sup> Cl (10 <sup>-14</sup> ) | [Cl] in sample (ppm)               | [ <sup>36</sup> Cl] (10 <sup>4</sup> atoms g <sup>-1</sup> ) | Age (years) <sup>a</sup>    | Mean age (years) |
|---------------------|-------------------|--------------------------|------------------------------------|---|------------------------------------|--|-----------------------------|------------------|
| G2                  |                   |                          |                                    |   |                                    |  |                             |                  |
| Ker-42              | 58.921            | 1.807                    | 11.88 ± 0.22                       | 4.97 ± 0.72   | 14.1                               | 3.36 ± 0.52  | 2340 ± 490 (480)            | 2620 ± 970       |
| Ker-44              | 64.436            | 1.807                    | 4.73 ± 0.11                        | 4.45 ± 0.48   | 72.4                               | 6.14 ± 0.76  | 3770 ± 750 (710)            |                  |
| Ker-45              | 66.252            | 1.810                    | 4.474 ± 0.087                      | 2.41 ± 0.35   | 84.1                               | 3.60 ± 0.59  | 1760 ± 570 (540)            |                  |
| G1                  |                   |                          |                                    |   |                                    |  |                             |                  |
| Ker-47              | 78.655            | 1.810                    | 5.59 ± 0.12                        | 16.7 ± 1.1  | 38.6                               | 14.8 ± 1.1   | 15 400 ± 1900 (1700)        | 14 300 ± 2300    |
| Ker-49              | 79.998            | 1.809                    | 8.86 ± 0.21                        | 19.1 ± 1.2  | 16.1                               | 11.28 ± 0.78   | 12 900 ± 1500 (1300)        |                  |
| Ker-50              | 68.34             | 1.817                    | 14.03 ± 0.37                       | 19.7 ± 1.4  | 9.7                                | 11.38 ± 0.86   | 12 800 ± 1600 (1500)        |                  |
| Ker-56              | 62.806            | 1.819                    | 6.18 ± 0.18                        | 12.2 ± 1.1  | 39.1                               | 12.1 ± 1.2   | 11 800 ± 1700 (1500)        |                  |
| <i>Ker-57</i>       | <i>69.965</i>     | <i>1.811</i>             | <i>12.66 ± 0.35</i>                | <i>39.8 ± 2.6</i>                                       | <i>10.9</i>                        | <i>23.3 ± 1.5</i>  | <i>30 100 ± 3600 (2900)</i> |                  |
| Ker-58              | 81.757            | 1.815                    | 9.7 ± 1.1                          | 18.4 ± 4.9  | 13.6                               | 10.2 ± 2.8   | 12 700 ± 3800 (3700)        |                  |
| Ker-65              | 78.533            | 1.813                    | 4.65 ± 0.12                        | 10.85 ± 0.92  | 62.7                               | 13.0 ± 1.4   | 12 500 ± 1900 (1700)        |                  |
| Ker-66              | 82.264            | 1.817                    | 5.90 ± 0.16                        | 16.9 ± 1.3  | 32.8                               | 13.5 ± 1.2   | 16 200 ± 2100 (1900)        |                  |
| Ker-67              | 76.263            | 1.823                    | 5.22 ± 0.14                        | 15.3 ± 1.2  | 47.1                               | 15.4 ± 1.5   | 17 500 ± 2500 (2200)        |                  |
| Ker-68              | 72.835            | 1.812                    | 9.90 ± 0.22                        | 21.4 ± 1.4  | 14.9                               | 13.17 ± 0.90   | 16 900 ± 2000 (1800)        |                  |
| Blanks <sup>b</sup> |                   |                          |                                    |   | Total atoms Cl (10 <sup>17</sup> ) | Total atoms <sup>36</sup> Cl (10 <sup>4</sup> )              |                             |                  |
| Bk1                 | -                 | 1.623                    | 300.7 ± 5.2                        | 0.395 ± 0.081   | 2.60 ± 0.14                        | 11.1 ± 2.3   | -                           | -                |
| Bk2                 | -                 | 1.610                    | 261.5 ± 3.0                        | 0.379 ± 0.085   | 3.16 ± 0.16                        | 10.6 ± 2.4   | -                           | -                |
| Bk3                 | -                 | 1.760                    | 222.9 ± 1.3                        | 0.361 ± 0.078   | 4.30 ± 0.21                        | 11.0 ± 2.4   | -                           | -                |
| Mean <sup>c</sup>   | -                 | -                        | -                                  | -   | 3.36 ± 0.17                        | 10.9 ± 2.4   | -                           | -                |

<sup>a</sup> Age uncertainties are reported at the 1σ level and were calculated through full propagation of analytical and production rate errors. Numbers in parentheses are analytical uncertainties only.

<sup>b</sup> Bk1, Bk2 and Bk3 were processed with samples from Jomelli *et al.* (2017, 2018).

<sup>c</sup> Samples were corrected with this mean.

internal comparison between the ages, the individual ages are indicated with their analytical uncertainties in the text and figures. Arithmetic means are mentioned with their full uncertainties to allow for comparison with other palaeorecords. This full error results for each age population from the calculation of the standard deviation added by quadrature propagation to the average analytical and production rate uncertainties. Each statistical population was tested using a  $\chi^2$  test, thus enabling the identification of potential outliers.

During sampling, surfaces without direct evidence of frost, salt or wind impacts were preferred, as no quantitative erosion data are available for Kerguelen. A snow-cover correction did not seem necessary due to glaciological modelling showing a short modern annual duration of snow cover ( $\sim 1.5$  months at 90 m altitude and  $\sim 3$  weeks at 35 m altitude; Verfaillie *et al.* 2015, Favier *et al.* 2016).

## Results

The  $^{36}\text{Cl}$  CRE ages span from  $1760 \pm 540$  to  $17\,500 \pm 2200$  years. These ages are distributed among two statistically different populations corresponding to the two sets of moraines G1 and G2 on which the samples were collected (Fig. 2).

### $^{36}\text{Cl}$ CRE ages from G1 moraine boulders ( $n = 10$ )

The first outer and older group G1 is composed of several moraine ridges within up to 300 m distance from each other. Ker-56 and -57 were sampled on the external moraine ridge G1a located  $\sim 1.5$  km from the current ice front, and they are dated to  $11.8 \pm 1.5$  and  $30.1 \pm 2.9$  ka, respectively. The  $^{36}\text{Cl}$  CRE ages of Ker-47, -49, -50, -58, -65 and -66, collected on two moraine ridges G1b and G1c close to the external moraine, are  $15.4 \pm 1.7$ ,  $12.9 \pm 1.3$ ,  $12.8 \pm 1.5$ ,  $12.7 \pm 3.7$ ,  $12.5 \pm 1.7$  and  $16.2 \pm 1.9$  ka, respectively. Ker-67 and -68 were extracted from boulders on the inner ridge G1d and are dated to  $17.5 \pm 2.2$  and  $16.9 \pm 1.8$  ka, respectively. The nominal ages are not consistent with the stratigraphic order, but considering their internal (analytical) uncertainties, all ages except Ker-57 seem to belong to the sample population based on the  $\chi^2$  tests (Fig. 5). Ker-57 has been rejected as an outlier and might have been pre-exposed to cosmic rays in the past. G1 samples yield a mean age and full uncertainty of  $14.3 \pm 2.3$  ka ( $n = 9$ ) for the entire fossil moraine deposit. However, the  $^{36}\text{Cl}$  CRE age probability density plot (Fig. 5) shows two statistical subpopulations within the G1 group of samples. The older group is clustered around  $16.5 \pm 2.2$  ka ( $n = 4$ ), whereas the younger group is clustered around  $12.5 \pm 2.1$  ka ( $n = 5$ ).

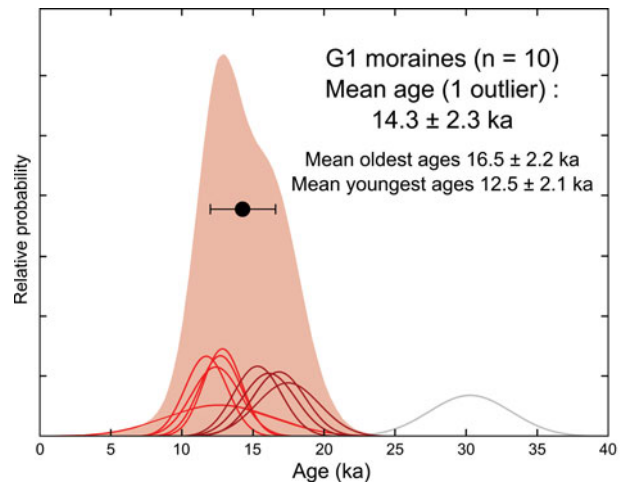


**Fig. 5.** Probability plots of  $^{36}\text{Cl}$  boulder cosmic-ray exposure (CRE) ages from the G1 moraine set. Individual  $^{36}\text{Cl}$  CRE ages are represented by thin red curves; the light grey curve is an outlier. The Gaussian curves of the individual ages only include the analytical uncertainties. The summed probability is presented by a red-shaded curve. The black circle represents the arithmetic mean of all individual ages except the outlier. Uncertainty of the arithmetic mean includes the standard deviation, analytical and production rate uncertainties. Also shown are the arithmetic means with their inferred full uncertainties of the two statistical subpopulations within the G1 group.

### $^{36}\text{Cl}$ CRE ages from G2 moraine boulders ( $n = 3$ )

Ker-42, -44 and -45 were sampled on two moraine ridges (G2a and G2b) close to the front position named group G2 (Figs 2 & 3). The  $^{36}\text{Cl}$  CRE ages are  $2.34 \pm 0.48$ ,  $3.77 \pm 0.71$  and  $1.76 \pm 0.54$  ka, respectively (Fig. 6). According to the  $\chi^2$  tests, these three samples from the G2 moraines are indistinguishable and yield a mean age of  $2.62 \pm 0.97$  ka.

## Discussion

The  $^{36}\text{Cl}$  CRE dating of the moraine groups G1 and G2 of Gentil Glacier provides new insights into the responses of debris-covered glaciers to climate variations in the Southern Hemisphere. It allows us, for the first time, to document the evolution of a debris-covered glacier on Kerguelen during the Late Glacial Period and the Holocene and to compare it to the previously investigated  $^{36}\text{Cl}$  chronologies of debris-free glaciers on the archipelago (Jomelli *et al.* 2017, 2018).

### Glacial fluctuation history of Gentil Glacier

Evidence of the Late Glacial glacier advance comes from  $^{36}\text{Cl}$  ages of boulders from several ridges of the fossil G1 moraine deposit. The individual ages are dispersed over

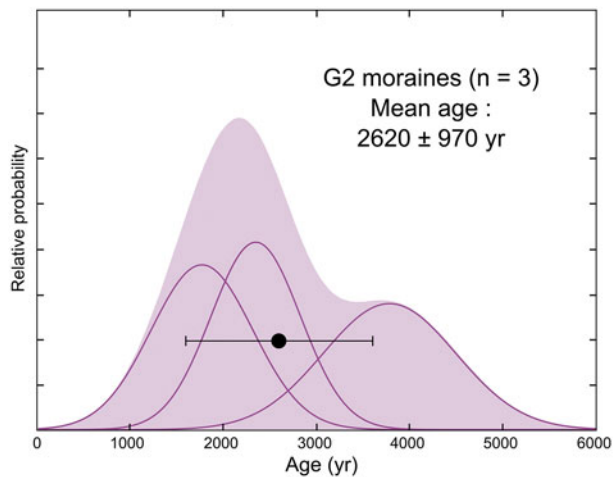


**Fig. 6.** Probability plots of  $^{36}\text{Cl}$  boulder cosmic-ray exposure (CRE) ages from the G2 moraine set. Individual  $^{36}\text{Cl}$  CRE ages are represented with thin purple curves. Note that the Gaussian curves of the individual ages only include the analytical uncertainties. The summed probabilities are presented by a purple-shaded curve. The black circle represents the arithmetic mean. Uncertainty of the arithmetic mean includes standard deviation and analytical and production rate (full) uncertainties.

a time span of several thousand years between  $\sim 18$  and  $\sim 12$  ka, and they are not in chronological order with regards to the position of the dated ridges. Considering the specific depositional processes leading to debris-covered glacier landforms and the related implications for their dating (see 'Methods' section), it is inferred that moraines G1a to G1d were formed during the same glacier advance period. Taken together, the age distribution of the G1 group exhibits two distinct subgroups, whose arithmetic means and full errors yield exposure ages of  $16.5 \pm 2.2$  and  $12.5 \pm 2.1$  ka, respectively (Fig. 5). This large age spread can be explained by the high probability of boulder pre-exposure and post-depositional processes in this specific setting, leading to variable exposure histories of the boulders within the same debris deposit (see 'Methods' section). Similarly to the interpretation of  $^{36}\text{Cl}$  boulder ages from a fossil rock glacier deposit in the Austrian Alps, which are subject to comparable dating challenges (Moran *et al.* 2016), it is thus proposed that: 1) the oldest  $^{36}\text{Cl}$  ages of the G1 moraine deposit are affected by some nuclide inheritance during boulder transportation before the glacier advance, 2) the youngest  $^{36}\text{Cl}$  ages most probably represent a late stabilization of the moraine deposit that postdates the glacial advance, notably accompanied by rotation and exhumation of debris during ice ablation, and 3) the glacier advance occurred sometime during this time span. We further assume that the best estimate for the

timing of this glacial advance is represented by the arithmetic mean and full error determined from the set of ages from the G1 moraine group ( $14.3 \pm 2.3$  ka), which largely overlaps with the ACR (14.5–12.9 ka) period, suggesting that glacier advance occurred during this period. The large G1 advance is probably not the oldest one in this area. Aerial photographs and field investigations revealed some moraine remains located at a distance of  $\sim 2.5$  km from the investigated moraines, suggesting older and larger ice extents. Dating of the three boulders from the G2 moraine deposit yielded ages spread between  $\sim 3.8$  and  $\sim 1.7$  ka, thus suggesting that another glacial advance occurred during the Late Holocene. Following the same rationale as above, we estimate the timing of this advance at  $2.62 \pm 0.97$  ka (arithmetic mean and full error).

Between the Late Glacial Period and the Late Holocene, the glacier evolution remains unknown. At least three moraine ridges can be identified between the two sets of dated ridges (Figs 2, 3 & 7). Samples from boulders of these moraines were used for an unsuccessful trial of *in situ* cosmogenic  $^3\text{He}$  dating, and no rock material remains from the field expedition for further  $^{36}\text{Cl}$  dating. However, we assume that two of these moraines, which are the closest to the G1 moraine group, belong to the Late Glacial glacier advance, because of the similarly eroded and revegetated topography. The other moraine ridge is located close to G2 in the area we described as inactive, which seems to still be ice-cored and is not yet revegetated. This moraine could belong to the Late Holocene advance dated on the G2 moraines or to an anterior one.

Pumice stones deposited at several locations on the western part of the archipelago during a volcanic eruption dated to the beginning of the last millennium (Arnaud *et al.* unpublished data 2016) were observed on the G1 and G2 moraines and between them, but not on morainic bulges upstream of G2 ridges. It is thus suggested that the glacier advanced again, bulging new ridges after this volcanic eruption (i.e. during the last millennium).

#### *Glacier evolution on Kerguelen Archipelago: the debris-covered Gentil Glacier in comparison with debris-free glaciers*

Kerguelen Archipelago offers an opportunity to compare the possible synchrony or asynchrony between the two different glaciers types (debris-covered *vs* debris-free). Despite the limited number of dated moraines and high degree of uncertainties in the ages related to the method and the specific challenges in dating boulders of debris-covered glaciers, the distribution of the  $^{36}\text{Cl}$  ages covering the Late Glacial Period from Gentil Glacier overlaps with other debris-free glacier chronologies such



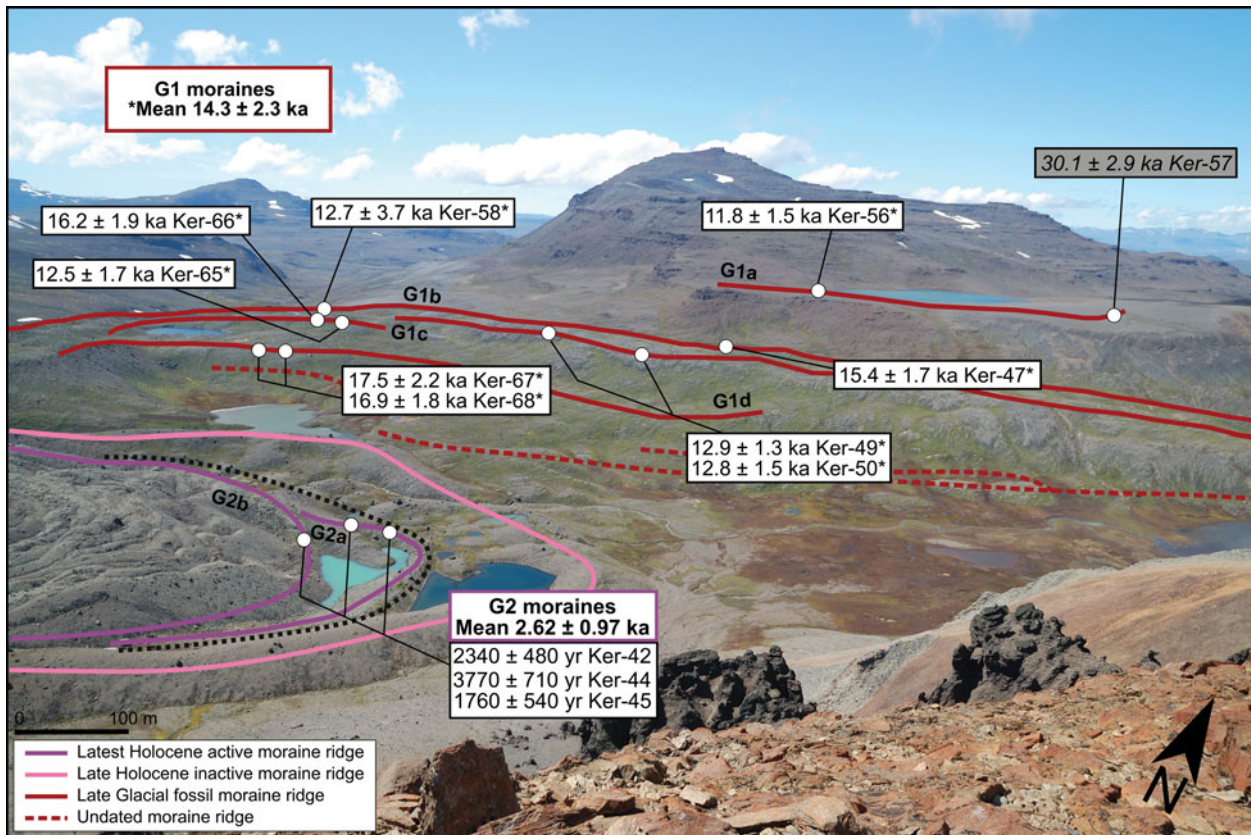


**Fig. 7.** Location of  $^{36}\text{Cl}$  cosmic-ray exposure (CRE) ages with their arithmetic means. The  $1\sigma$  uncertainties in the individual  $^{36}\text{Cl}$  CRE boulder ages account for analytical uncertainties only, while the uncertainties in the means include the standard deviation, analytical and production rate uncertainties. Sample Ker-57 in italics was rejected as an outlier based on the  $\chi^2$  tests.

as Bontemps moraine formed by Explorateur Glacier and a smaller local glacier located on Presqu'île Jeanne D'Arc (Belvedere moraine) (Figs 8 & 9) (Jomelli *et al.* 2017). Comparing the timing of moraine formation at these different locations (i.e.  $13.6 \pm 1.5$  ka at Bontemps moraine,  $15.5 \pm 1.8$  ka at Belvedere moraine and  $14.3 \pm 2.3$  ka at Gentil G1 moraine) suggests a broadly synchronous advance (Fig. 9), potentially due to the same climate forcing.

Moreover, none of the existing glacier chronologies provides evidence of large advances between the Late Glacial Period and the Late Holocene. The advance of Gentil Glacier at  $\sim 2.6$  ka has so far not been directly documented for debris-free glaciers of the archipelago. In addition, the age and standard deviation of G2 moraine ( $2.62 \pm 0.97$  ka) is distinguishable from the age of the last-millennium moraine of Ampere Glacier ( $0.70 \pm 0.32$  ka) (Jomelli *et al.* 2017), suggesting an advance of Gentil Glacier that occurred  $\sim 2$  ka earlier than that of Ampere Glacier. However, this does not exclude the theory that these glaciers experienced a comparable trend, as moraines of Ampere Glacier may have been overrun by the more recent advances. In addition, Gentil Glacier might also have experienced a

glacial advance during the last millennium, as is suggested by the observed lack of pumice stones on moraine ridges upstream of the G2 moraine set.

#### Climate sensitivity

CIC has experienced a glacial shrinkage over the last few decades (Favier *et al.* 2016) owing to a dramatic drought occurring since the mid-1960s in the archipelago. To put this observation into a long-term context, we aim to understand whether the unusual current Kerguelen glacier sensitivity to precipitation changes differs from the past responses of the different types of glaciers to climate fluctuations at a regional scale.

The recent evolution of debris-covered glaciers at Kerguelen is difficult to assess because remote-sensing techniques, which are often used to determine surface mass balance through elevation changes of the glacial tongue (Vincent *et al.* 2016, Brun *et al.* 2018), are difficult to apply here due to a consistent high degree of cloud cover at Kerguelen. Without mass and energy balance measurements in the field, a comparison between debris-free and debris-covered ice wastage on the archipelago is difficult to perform.

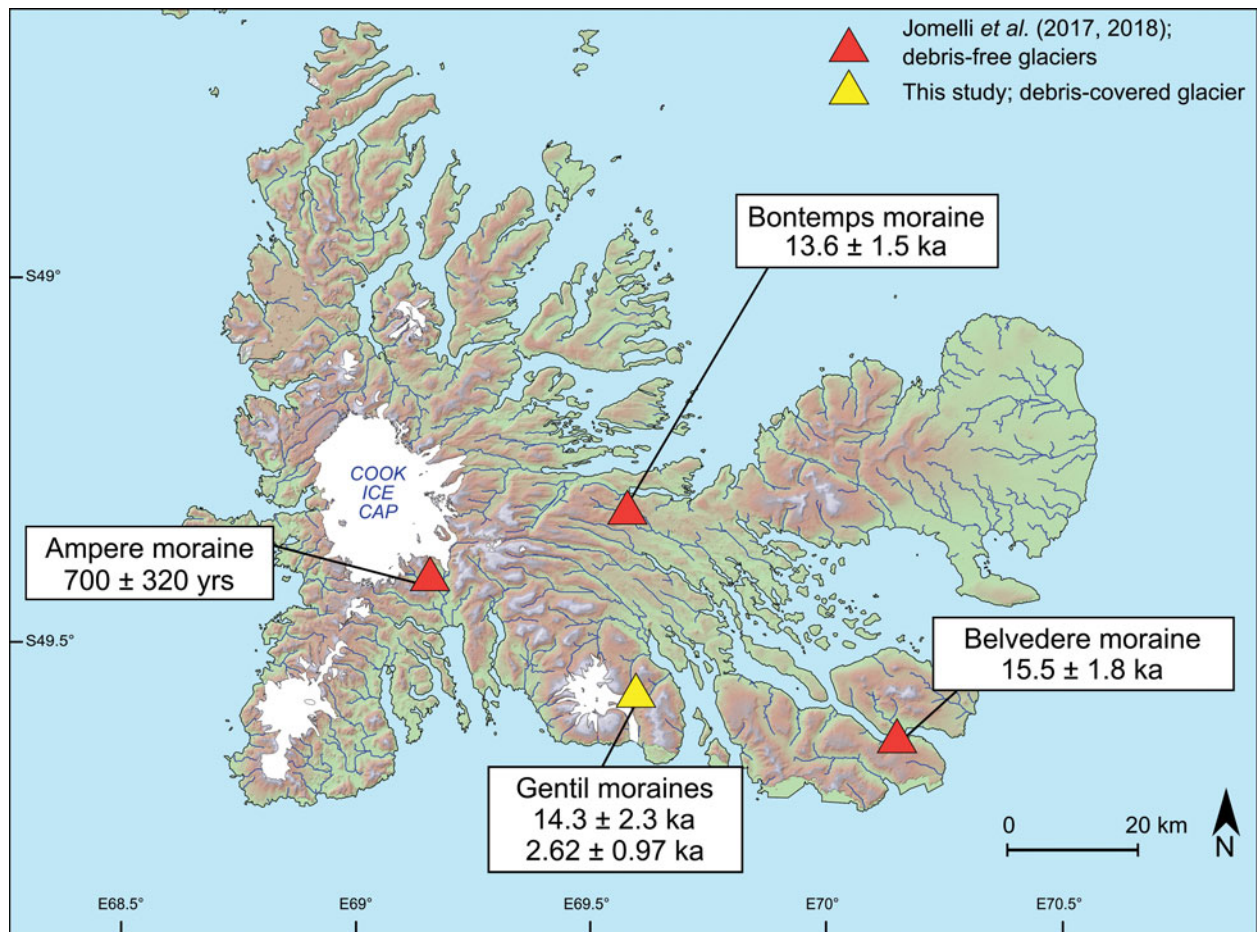


**Fig. 8.** Summary of  $^{36}\text{Cl}$  cosmic-ray exposure (CRE) ages covering the investigated period obtained at different sample sites (this study and Jomelli *et al.* 2017, 2018). Reported mean  $^{36}\text{Cl}$  CRE boulder ages account for the standard deviation, analytical and production rate uncertainties.

Palaeoglacial studies based on approaches such as  $^{36}\text{Cl}$  CRE dating represent a useful tool to compare the responses of both glacier types to multi-millennial climate variation. Based on the results presented here, it is postulated that Gentil Glacier has been sensitive to multi-millennial climate fluctuations, with behaviour that is broadly synchronous with debris-free glaciers on Kerguelen Archipelago, at least since the Late Glacial Period, most probably during the abrupt ACR event and probably also during the Holocene.

The ACR event was recorded in the WAIS Divide ice core (WDC) (Fig. 9b), where more depleted  $\delta^{18}\text{O}$  values and a decrease in snow accumulation rate (WAIS Divide Project Members 2013, Jomelli *et al.* 2017) are observed. This event influenced most of the Southern Hemisphere glaciers and even those in the tropical Andes (Jomelli *et al.* 2014). Some of the still-glaciated sub-Antarctic areas seem to have experienced more or less synchronous glacial advances in association with the ACR period (e.g. Putnam *et al.* 2010, Pedro *et al.* 2015, Darvill *et al.* 2016, Graham *et al.* 2017, Sagredo *et al.* 2018). In

addition, multi-proxy analysis of peat sequences on the eastern part of the archipelago indicate increased moisture and wind during the ACR (van der Putten *et al.* 2015), which supports the hypothesis of cold and wet conditions over Kerguelen owing to a potential shift of the westerlies belt (Jomelli *et al.* 2017). This would have led to glacial advances of debris-free as well as debris-covered glaciers, meaning that both types of Kerguelen glaciers were sensitive to the wide-ranging temperature fluctuations of the ACR (Jomelli *et al.* 2017, 2018).

The role of climate changes on Holocene glacier behaviour is more difficult to assess, as Late Holocene moraine deposits could reflect a climate-driven glacier advance and a non-climatic ice dynamics signature. The amplitude of temperature change documented from WDC records (WAIS Divide Project Members 2013) (Fig. 9b) remains rather limited compared to that of the ACR period. A general SAM-negative-like state (associated with higher precipitation) occurred during the Late Holocene (~2.7–0.1 ka) (Fig. 9c), as inferred from the Lago

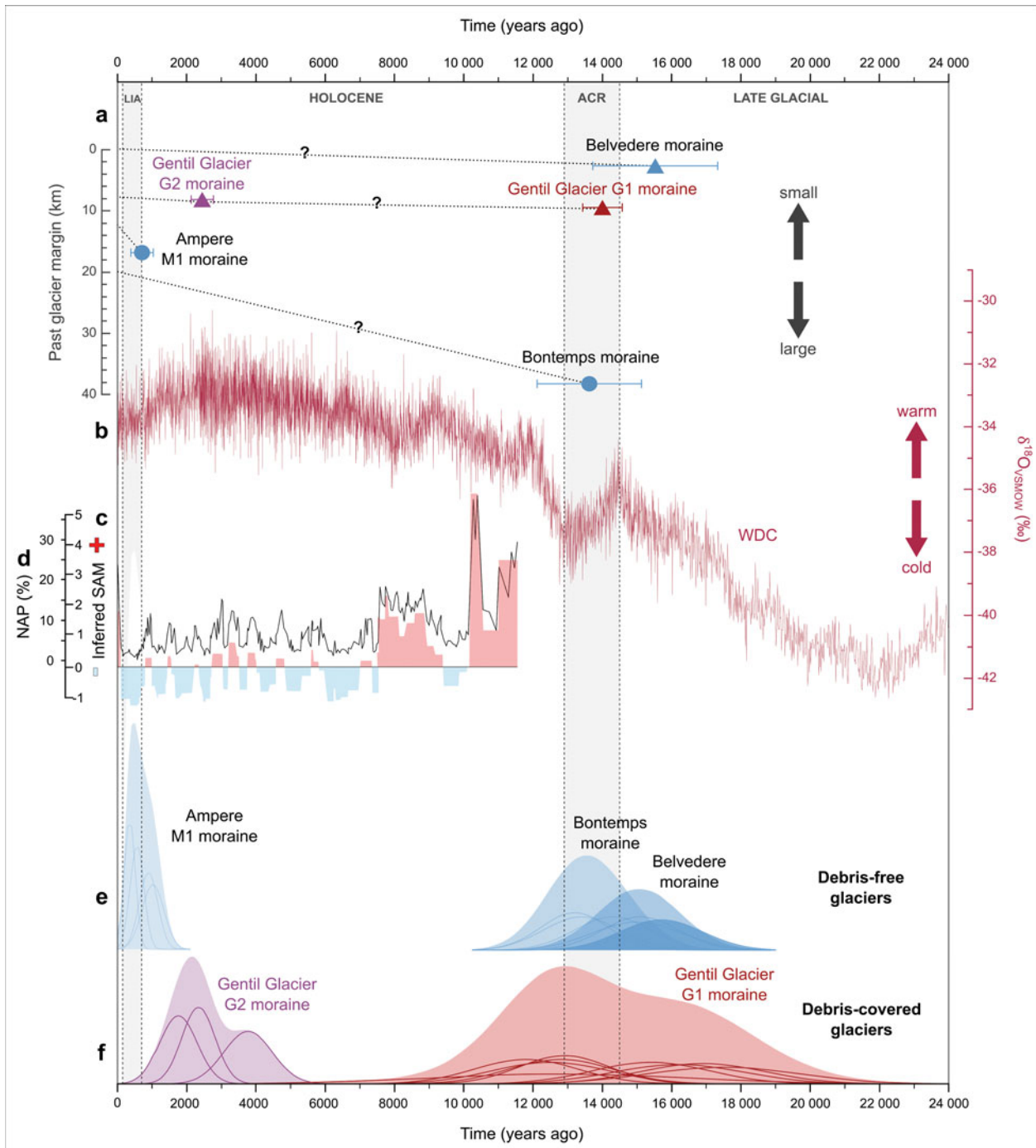


**Fig. 9.** Kerguelen palaeoglacier records compared with palaeoclimatic proxies. **a.** Glacier chronologies: Cook Ice Cap outlet glaciers (circles), local glaciers (triangles), Gentil debris-covered glacier (red, purple) and debris-free glaciers (blue). **b.** The water isotope ratio ( $\delta^{18}O_{VSMOW}$ ; red curve) from WAIS Divide Project Members (2013). **c.** Southern Annular Mode (SAM)-like states (red boxes = positive, blue boxes = negative), reconstructed from **d.** Lago Cipreses non-arboreal pollen (NAP; black curve) in Patagonia (Moreno *et al.* 2018). **e.** and **f.**  $^{36}Cl$  age probability density distributions with their analytical uncertainties (coloured curves) and summed probabilities (shaded areas) of debris-free glaciers (blue) (Jomelli *et al.* 2017, 2018) and debris-covered Gentil Glacier (red and purple). ACR = Antarctic Cold Reversal, WDC = WAIS Divide ice core. LIA = Little Ice Age.

Cipreses non-arboreal pollen record in Patagonia (Moreno *et al.* 2018) (Fig. 9d). This SAM-negative-like state supports more moisture during the Late Holocene that may have

partly compensated for possible warmer temperatures until 2.5 ka, thus suggesting the importance of precipitation in the formation of the G2 moraine set. This

behaviour would be supported by current observations that have revealed the major role of atmospheric drying related to high-index SAM conditions on current glacier retreat at Kerguelen (Verfaillie *et al.* 2015; Favier *et al.* 2016). The prominent role of precipitation in debris-covered glacier behaviour seems plausible, because supraglacial debris insulate the underlying glacier ice and possibly lower the glacier's sensitivity to low-ranging temperature changes. Increased precipitation and decreased temperature at ~2.5 ka may also have favoured glacier expansion of Ampere Glacier. In that case, it is possible that Ampere Glacier deposited moraines, which, however, would have been obliterated by more extensive advances during the last millennium. By contrast, Gentil Glacier has probably also expanded several times during the Late Holocene. However, the low terminus velocity of debris-covered glaciers and their external moraines being usually much bigger and broader than those of debris-free glaciers, owing to the high debris load, prevent the obliteration of earlier moraine ridges. In addition, given that Gentil Glacier is a marginal glacier lobe of Buffon Glacier, its ice dynamics might have been partly controlled by the behaviour of the ocean-terminating main glacier tongue, leading to fluctuations that are less directly related to climate changes than those of Ampere Glacier.

## Conclusion

This study provides new insights into the multi-millennial evolution of debris-covered glaciers, which are very scarce in the Southern Hemisphere. The chronology established here of Gentil Glacier on Kerguelen Archipelago, constrained by *in situ*-produced  $^{36}\text{Cl}$  CRE dating, allows for documenting periods of large advances of this debris-covered glacier and for comparing them to existing chronologies of debris-free Kerguelen glaciers (Jomelli *et al.* 2017, 2018). Evidence of two glacial advances of Gentil Glacier is provided: the first during the Late Glacial Period (~14.3 ka), which could coincide with the ACR event, and the second during the Late Holocene (~2.6 ka). As debris-free glaciers experienced advances that can probably also be assigned to the ACR, this broadly synchronous behaviour suggests that both debris-free and debris-covered glaciers were sensitive to the multi-millennial temperature fluctuations recorded in the WDC (WAIS Divide Project Members 2013). The Late Holocene advance experienced by Gentil Glacier has not yet been observed for the debris-free glaciers. This advance could be a specific response of debris-covered glaciers to a significant precipitation increase resulting from infra-millennial SAM-like changes. Thus, the debris-covered Gentil Glacier was probably sensitive to large-amplitude temperature changes, but also to precipitation changes. On the basis of current qualitative

observations and palaeoglacial investigations, it appears that all types of Kerguelen glaciers have been sensitive to the same climate forcings, but the amplitudes of their glacial responses might be distinct.

## Supplemental material

A supplemental methods section and two supplemental tables will be found at <https://doi.org/10.1017/S0954102020000541>.

## Acknowledgements

We are thankful to the two anonymous reviewers for their positive and constructive comments.

## Author contributions

VJ, DV, VF and AG conducted the fieldwork on the islands. IS and FM participated in producing the cosmogenic data. GA, DLB and KK (ASTER Team) performed accelerator mass spectrometry measurements. JC, IS and VJ interpreted the cosmogenic ages; JC, VJ and IS prepared the figures. JC, VJ, IS, DV, VF, FB, AG and DLB contributed to writing the paper.

## Financial support

This work has received financial support from the LabEx DynamiTe (ANR-11-LABX-0046) Les Envahisseurs as part of the 'Investissements d'Avenir' programme. This paper was also supported by the French INSU LEFE Glacépreker project and by the IPEV Kesaaco 1048 project. The  $^{36}\text{Cl}$  measurements were performed at the ASTER national accelerator mass spectrometry facility (CEREGE, Aix-en-Provence) that is supported by the INSU/CNRS, the ANR through the 'Projets thématiques d'excellence' programme for the 'Equipements d'excellence' ASTER-CEREGE action and IRD.

## Details of data deposit

These  $^{36}\text{Cl}$  data will be found on the open-access repository of the informal cosmogenic-nuclide exposure-age database (ICE-D: Alpine; <http://alpine.ice-d.org>).

## References

- BERTHIER, E., LE BRIS, R., MABILEAU, L., TESTUT, L. & RÉMY, F. 2009. Ice wastage on the Kerguelen Islands (49°S, 69°E) between 1963 and 2006. *Journal of Geophysical Research - Earth Surface*, **114**, 10.1029/2008JF001192.
- BRUN, F., WAGNON, P., BERTHIER, E., JOMELLI, V., MAHARJAN, S.B., SHRESTHA, F. & KRAAIJENBRINK, P.D.A. 2019. Heterogeneous influence of glacier morphology on the mass balance variability in High Mountain Asia. *Journal of Geophysical Research: Earth Surface*, **124**, 10.1029/2018JF004838.

- BRUN, F., WAGNON, P., BERTHIER, E., SHEA, J.M., IMMERZEEL, W.W., KRAAIJENBRINK, P.D.A., *et al.* 2018. Ice cliff contribution to the tongue-wide ablation of Changri Nup Glacier, Nepal, central Himalaya. *The Cryosphere*, **12**, 10.5194/tc-12-3439-2018.
- DARVILL, C.M., BENTLEY, M.J., STOKES, C.R. & SHULMEISTER, J. 2016. The timing and cause of glacial advances in the southern mid-latitudes during the last glacial cycle based on a synthesis of exposure ages from Patagonia and New Zealand. *Quaternary Science Reviews*, **149**, 10.1016/j.quascirev.2016.07.024.
- EVANS, D.J.A. 2009. Controlled moraines: origins, characteristics and palaeoglaciological implications. *Quaternary Science Reviews*, **28**, 10.1016/j.quascirev.2008.10.024.
- FAVIER, V., VERFAILLIE, D., BERTHIER, E., MENEGOUZ, M., JOMELLI, V., KAY, J.E., *et al.* 2016. Atmospheric drying as the main driver of dramatic glacier wastage in the southern Indian Ocean. *Scientific Reports*, **6**, 10.1038/srep32396.
- FERNÁNDEZ-FERNÁNDEZ, J.M., PALACIOS, D., ANDRÉS, N., SCHIMMELPFENNIG, I., TANARRO, L.M., BRYNJÓLFSSON, S., *et al.* 2020. Constraints on the timing of debris-covered and rock glaciers: an exploratory case study in the Hólar area, northern Iceland. *Geomorphology*, **361**, 10.1016/j.geomorph.2020.107196.
- FERNÁNDEZ-FERNÁNDEZ, J.M., PALACIOS, D., GARCÍA-RUIZ, J.M., ANDRÉS, N., SCHIMMELPFENNIG, I., GÓMEZ-VILLAR, A., *et al.* 2017. Chronological and geomorphological investigation of fossil debris-covered glaciers in relation to deglaciation processes: a case study in the Sierra de La Demanda, northern Spain. *Quaternary Science Reviews*, **170**, 10.1016/j.quascirev.2017.06.034.
- FRENOT, Y., GLOAGUEN, J.-C., VAN DE VIJVER, B. & BEYENS, L. 1997. Datation de quelques sédiments tourbeux holocènes et oscillations glaciaires aux îles Kerguelen. *Comptes Rendus de l'Académie des Sciences - Serie III*, **320**, 10.1016/S0764-4469(97)84712-9.
- GRAHAM, A.G.C., KUHN, G., MEISEL, O., HILLENBRAND, C.-D., HODGSON, D.A., EHRMANN, W., *et al.* 2017. Major advance of South Georgia glaciers during the Antarctic Cold Reversal following extensive sub-Antarctic glaciation. *Nature Communications*, **8**, 10.1038/ncomms14798.
- HEYMAN, J., STROEVEN, A.P., HARBOR, J.M. & CAFFEE, M.W. 2011. Too young or too old: evaluating cosmogenic exposure dating based on an analysis of compiled boulder exposure ages. *Earth and Planetary Science Letters*, **302**, 10.1016/j.epsl.2010.11.040.
- JOMELLI, V., FAVIER, V., VUILLE, M., BRAUCHER, R., MARTIN, L., BLARD, P.-H., *et al.* 2014. A major advance of tropical Andean glaciers during the Antarctic Cold Reversal. *Nature*, **513**, 10.1038/nature13546.
- JOMELLI, V., MOKADEM, F., SCHIMMELPFENNIG, I., CHAPRON, E., RINTERKNECHT, V., FAVIER, V., *et al.* 2017. Sub-Antarctic glacier extensions in the Kerguelen region (49°S, Indian Ocean) over the past 24,000 years constrained by <sup>36</sup>Cl moraine dating. *Quaternary Science Reviews*, **162**, 10.1016/j.quascirev.2017.03.010.
- JOMELLI, V., SCHIMMELPFENNIG, I., FAVIER, V., MOKADEM, F., LANDAIS, A., RINTERKNECHT, V., *et al.* 2018. Glacier extent in sub-Antarctic Kerguelen archipelago from MIS 3 period: evidence from <sup>36</sup>Cl dating. *Quaternary Science Reviews*, **183**, 10.1016/j.quascirev.2018.01.008.
- KÄÄB, A., BERTHIER, E., NUTH, C., GARDELLE, J. & ARNAUD, Y. 2012. Contrasting patterns of early twenty-first-century glacier mass change in the Himalayas. *Nature*, **488**, 10.1038/nature11324.
- MAYR, E. & HAGG, W. 2019. Debris-covered glaciers. In HECKMANN, T. & MORCHE, D., eds. *Geomorphology of proglacial systems. Landform and sediment dynamics in recently deglaciated alpine landscapes*. Cham: Springer International Publishing, 59–71.
- MORAN, A.P., IVY OCHS, S., VOCKENHUBER, C. & KERSCHNER, H. 2016. Rock glacier development in the Northern Calcareous Alps at the Pleistocene-Holocene boundary. *Geomorphology*, **273**, 10.1016/j.geomorph.2016.08.017.
- MORENO, P.I., VILANOVA, I., VILLA-MARTÍNEZ, R., DUNBAR, R.B., MUCCIARONE, D.A., KAPLAN, M.R., *et al.* 2018. Onset and evolution of Southern Annular Mode-like changes at centennial timescale. *Scientific Reports*, **8**, 10.1038/s41598-018-21836-6.
- OJHA, S., FUJITA, K., SAKAI, A., NAGAI, H. & LAMSAL, D. 2017. Topographic controls on the debris-cover extent of glaciers in the Eastern Himalayas: regional analysis using a novel high-resolution glacier inventory. *Quaternary International*, **455**, 10.1016/j.quaint.2017.08.007.
- PEDRO, J.B., BOSTOCK, H.C., BITZ, C.M., HE, F., VANDERGOES, M.J., STEIG, E.J., *et al.* 2015. The spatial extent and dynamics of the Antarctic Cold Reversal. *Nature Geoscience*, **9**, 10.1038/ngeo2580.
- PUTNAM, A.E., DENTON, G.H., SCHAEFER, J.M., BARRELL, D.J.A., ANDERSEN, B.G., FINKEL, R.C., *et al.* 2010. Glacier advance in southern middle-latitudes during the Antarctic Cold Reversal. *Nature Geoscience*, **3**, 10.1038/ngeo962.
- RAUB, B., RACOVITEANU, A., KHALSA, S.J.S., HELM, C., ARMSTRONG, R. & ARNAUD, Y. 2007. The GLIMS geospatial glacier database: a new tool for studying glacier change. *Global and Planetary Change*, **56**, 10.1016/j.gloplacha.2006.07.018.
- RUDOLPH, E.M., HEDDING, D.W., FABEL, D., HODGSON, D.A., GHEORGHIU, D.M., SHANKS, R. & NEL, W. 2020. Early glacial maximum and deglaciation at sub-Antarctic Marion Island from cosmogenic <sup>36</sup>Cl exposure dating. *Quaternary Science Reviews*, **231**, 10.1016/j.quascirev.2020.106208.
- SAGREDO, E.A., KAPLAN, M.R., ARAYA, P.S., LOWELL, T. V., ARAVENA, J.C., MORENO, P.I., *et al.* 2018. Trans-pacific glacial response to the Antarctic Cold Reversal in the southern mid-latitudes. *Quaternary Science Reviews*, **188**, 10.1016/j.quascirev.2018.01.011.
- SALERNO, F., THAKURI, S., TARTARI, G., NUIMURA, T., SUNAKO, S., SAKAI, A. & FUJITA, K. 2017. Debris-covered glacier anomaly? Morphological factors controlling changes in the mass balance, surface area, terminus position, and snow line altitude of Himalayan glaciers. *Earth and Planetary Science Letters*, **471**, 10.1016/j.epsl.2017.04.039.
- SCHERLER, D., WULF, H. & GORELICK, N. 2018. Global assessment of supraglacial debris-cover extents. *Geophysical Research Letters*, **45**, 10.1029/2018GL080158.
- THOMPSON, D.W.J., SOLOMON, S., KUSHNER, P.J., ENGLAND, M.H., GRISE, K.M. & KAROLY, D.J. 2011. Signatures of the Antarctic ozone hole in Southern Hemisphere surface climate change. *Nature Geoscience*, **4**, 10.1038/ngeo1296.
- THOST, D.E. & TRUFFER, M. 2008. Glacier recession on Heard Island, southern Indian Ocean. *Arctic, Antarctic, and Alpine Research*, **40**, 10.1657/1523-0430(06-084)[THOST]2.0.CO;2.
- VAN DER PUTTEN, N., VERBRUGGEN, C., BJÖRCK, S., MICHEL, E., DISNAR, J.-R., CHAPRON, E., *et al.* 2015. The Last termination in the South Indian Ocean: a unique terrestrial record from Kerguelen Islands (49°S) situated within the Southern Hemisphere westerly belt. *Quaternary Science Reviews*, **122**, 10.1016/j.quascirev.2015.05.010.
- VERFAILLIE, D., FAVIER, V., GALLÉE, H., FETTWEIS, X., AGOSTA, C. & JOMELLI, V. 2019. Regional modeling of surface mass balance on the Cook Ice Cap, Kerguelen Islands (49°S, 69°E). *Climate Dynamics*, **53**, 10.1007/s00382-019-04904-z.
- VERFAILLIE, D., FAVIER, V., DUMONT, M., JOMELLI, V., GILBERT, A., BRUNSTEIN, D., *et al.* 2015. Recent glacier decline in the Kerguelen Islands (49°S, 69°E) derived from modeling, field observations, and satellite data. *Journal of Geophysical Research - Earth Surface*, **120**, 10.1002/2014JF003329.
- VINCENT, C., WAGNON, P., SHEA, J.M., IMMERZEEL, W.W., KRAAIJENBRINK, P., SHRESTHA, D., *et al.* 2016. Reduced melt on debris-covered glaciers: investigations from Changri Nup Glacier, Nepal. *The Cryosphere*, **10**, 10.5194/tc-10-1845-2016.
- WAIS Divide Project Members. 2013. Onset of deglacial warming in West Antarctica driven by local orbital forcing. *Nature*, **500**, 10.1038/nature12376.